Research Paper: International Journal of Hydrogen Energy

Title:
A comparison study into low leak rate buoyant gas dispersion in a small fuel cell enclosure using plain and louvre vent passive ventilation schemes

Authors: Ghatauray, T.S.*, Ingram, J.M., Holborn, P.G.

Explosion and Fire Research Group, School of Engineering, London South Bank University (LSBU), Borough Road, London, SE1 0AA, UK, Tel: 07815 932779

*Corresponding author: ghataurt@lsbu.ac.uk

Abstract
Hydrogen, producing electricity in fuel cells, is a versatile energy source, but with risks associated with flammability. Fuel cells use enclosures for protection which need ventilating to remove hydrogen emitted during normal operation or from supply system leaks. Passive ventilation, using buoyancy driven flow is preferred to mechanical systems. Performance depends upon vent design, size, shape, position and number. Vents are usually plain rectangular openings, but environmentally situated enclosures use louvres for protection. The effect of louvres on passive ventilation is not clear and has therefore been examined in this paper. Comparison 'same opening area' louvre and plain vent tests were undertaken using a 0.144 m^3 enclosure with opposing upper and lower vents and helium leaking from a 4 mm nozzle on the base at rates from 1 to 10 lpm, simulating a hydrogen leak. Louvres increased stratified level helium concentrations by typically in excess of 15 %. The empirical data obtained was also used in a validation exercise with a SolidWorks: Flow Simulation CFD model, which provided a good qualitative representation of flow behaviour and close empirical data correlations.

Keywords
- Hydrogen safety,
- Passive ventilation
- Buoyant gas
- Louvre vent
- Helium
- SolidWorks: Flow Simulation CFD

Nomenclature and units

nlpm	Normal litre per minute
lpm	Litre per minute
C_d	Discharge coefficient

Abbreviations

STP	Standard temperature and pressure
LFL	Lower flammable limit (Hydrogen = 4%)
CFD	Computational fluid dynamics

1.0 Introduction

There is a global move away from fossil fuel dependence and its replacement with a distributed energy system based around renewable energy sources. A 'Hydrogen Economy' is promoted as a transition measure that will support the development of the new renewable energy infrastructure. The hydrogen economy though will only succeed if concerns relating to hydrogen production, storage, transportation and safe conversion to a viable energy source are resolved.

Hydrogen fuel cells are a key part of the initiative being used at a variety of scales to provide distributed energy. Low power fuel cells, housed in small protective enclosures, are likely to become widely used

in domestic and commercial applications. However, because fuel cells emit small amounts of hydrogen and there is the possibility of a leak from supply pipes, the enclosures represent a potential hydrogen confinement hazard. Hydrogen's wide flammable range (4-75%) means that explosive mixtures can quickly develop, so effective ventilation is needed to maintain safe concentrations. Passive hydrogen removal research is motivated by accident prevention and the need to understand hydrogen's behaviour in hazardous scenarios [1]. Hydrogen accidents begin with evolution/leaks in air, followed by ignition, fire or deflagration with thermal/pressure effects which can threaten life and property. Confinement scenarios have more serious outcomes since significant explosion overpressures can be developed [2]. Confidence in hydrogen safety will support fuel cell use and progression to the wider use of renewables.

Deployment of small low power fuel cells is becoming popular in remote locations to replace diesel generators, powering lighting and cellular telephone towers. These installations are exposed to environmental conditions and require protective enclosures. Ventilation design in these enclosures is important so that water ingress is prevented, the effect of wind forces [3] is effectively managed and the possibility of vent blockages, e.g. by foliage, is accounted for. Vent obstructions impede air flow through the enclosure and can lead to increased concentrations of unvented hydrogen. Meshes may also be necessary to prevent rodents and insects from gaining access and damaging pipes and circuitry.

Enclosure ventilation solutions require complex safety considerations and design insight. Natural ventilation is the flow of air through a confined volume due to wind, thermal and pressure differences. An extensive review [4] of the conditions responsible for producing natural ventilation found that density differences and buoyancy are the driving forces in scenarios where wind forces are absent, which is the case in some enclosure deployments. Two distinct regimes of natural ventilation were also identified: (i) mixing ventilation (e.g. via a single upper vent, which allows an exchange of air through a two-way flow) producing an (approximately) uniform condition throughout the interior of an enclosure and (ii) displacement ventilation (e.g. via two vents one located near the top and one near the bottom, with air flow in one direction) where a stratified condition develops with distinct layers. Natural ventilation theory developed for buildings [5] [6] has been applied to buoyant gas enclosure scenarios.

The presence of a buoyant gas in the ventilation flow has been shown to have an effect upon the flow dynamics. As such a distinction has been made between 'natural ventilation', applicable to the flow of air only and 'passive ventilation' which occurs when a buoyant gas such as hydrogen mixes with the air in the ventilation flow. It has been determined that for natural ventilation of air in an enclosure with one vent, the neutral plane (where internal pressure is equal to external air pressure) is located half-way up the opening (i.e. by making the approximation that the volumetric flow rates of air entering and leaving through the vent are equal). However, this is not necessarily the case for a passive ventilation scenario involving the release of a lighter than air gas (e.g. air and hydrogen), where for sufficiently high release rates, the neutral plane can be positioned anywhere between the half-way point and the bottom of the vent [7].

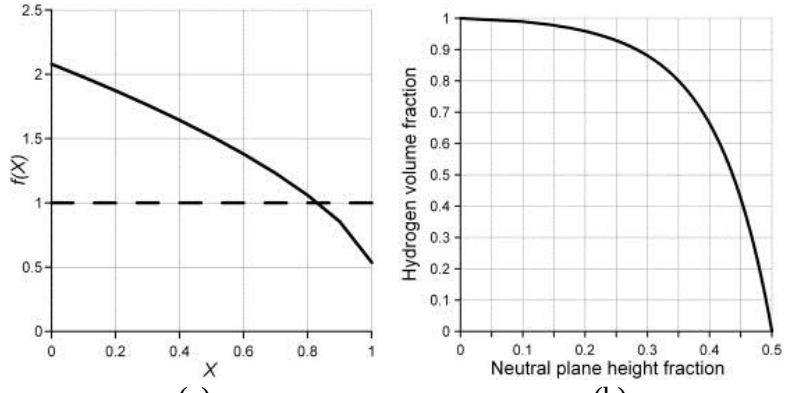

Figure 1 (a) function *f(X)* for passive ventilation (solid line) and for natural ventilation (dash line). (b) hydrogen volume fraction (*X*) in enclosure as a function of neutral plane height fraction [7].

Figure 1(a), taken from [7], compares the predictive capability of equations for passive and natural ventilation, showing the change of *f(X)* – the correction factor for passive ventilation - with the hydrogen volumetric fraction in air, *X*. It shows that if the natural ventilation equations were applied to a passive ventilation scenario it would under predict at low volumetric hydrogen concentrations and over predict for very high ones. Figure 1(b), also from [7], shows a functional dependence between the vent neutral plane height and hydrogen mole fraction. For a natural ventilation scenario where the hydrogen volume fraction is zero the neutral plane divides the vent equally for incoming and outgoing air. As the hydrogen volume fraction in the enclosure increases, associated with an increase in leak rate the neutral plane becomes lower. This phenomenon has relevance to other ventilation scenarios. Hydrogen management through passive venting is viable due to its inherent reliability and hydrogen's suitability as a buoyant gas [8], so there is confidence in the application of these concepts to small fuel cell enclosures to manage concentrations below the LFL [9].

Environmentally situated enclosures use louvre vents (angled horizontal bars across the ventilation opening for protection). However, the ventilation performance of vents with louvres compared with plain rectangular vents is not clear. Previous passive ventilation studies have typically used plain, vertical, rectangular vents for which the discharge coefficient (C_d), a measure of vent flow resistance, can be readily determined. When louvres are fitted to a vent, the opening is no longer vertical, but angled close to the horizontal and it may also have rounded edges. These louvre vent characteristics will influence the C_d and the enclosure flow regime. Hence, data from plain vent tests cannot be simply applied to vents with louvres of the same opening area. Comparison tests were conducted to determine the extent of flow impairment. This investigation uses simplified louvre extensions to test their affect. Computational fluid dynamics (CFD) has capability in predicting hydrogen dispersion and can inform passive ventilation system design, with validated CFD models saving development time in engineering applications. SolidWorks Flow Simulation CFD is untested in this field, so this investigations empirical data has been used in a validation process for the code.

2.0 Method: Experimental

In this study, a test rig was constructed consisting of Perspex outer chamber 1m x 1m x 2m long, intended to prevent draughts affecting experimental ventilation flow. The outer chamber contained a 0.144 m^3 plywood (5 mm) structure (0.6 m x 0.6 m x 0.4 m) (Figure 2), which represented a ventilated fuel cell enclosure, designed to facilitate the investigation of vent design on passive buoyant gas ventilation behaviour. A cross flow displacement ventilation vent arrangement was incorporated, with opposing upper and lower plain rectangular ventilation openings (20mm high x 360mm wide).

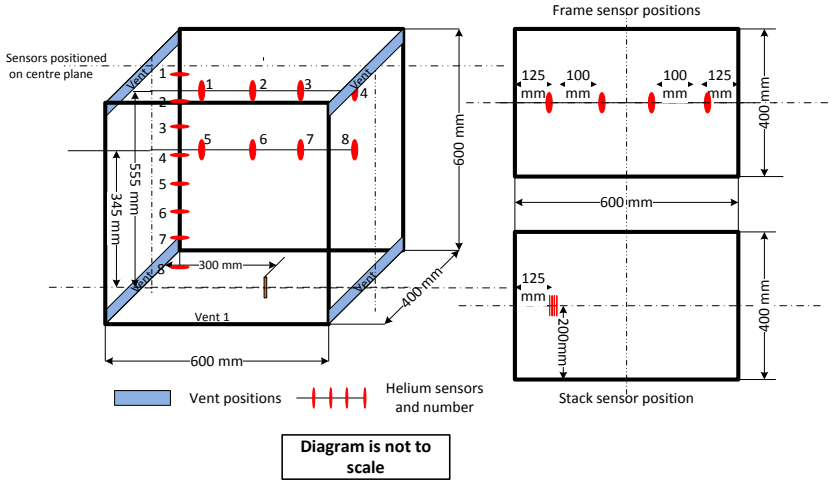

Figure 2 Experimental schematic showing the position of helium sensors and vents

For the louvre vent tests, the plain vents were adapted with two 10mm horizontal louvre blade extensions across the full vent width. These were fabricated from stiff cardboard with one positioned at the vertical mid-point and one positioned at the top of the vent (Figure 3). The louvre and plain vents

were fabricated with the same vertical opening area, so any difference in passive ventilation flow between the two arrangements could therefore be attributed to a change in flow resistance or discharge coefficient, due to the presence of the horizontal louvre extensions. A horizontal extension is the simplest representation of a louvre. Louvres used on commercial installations are more restrictive.

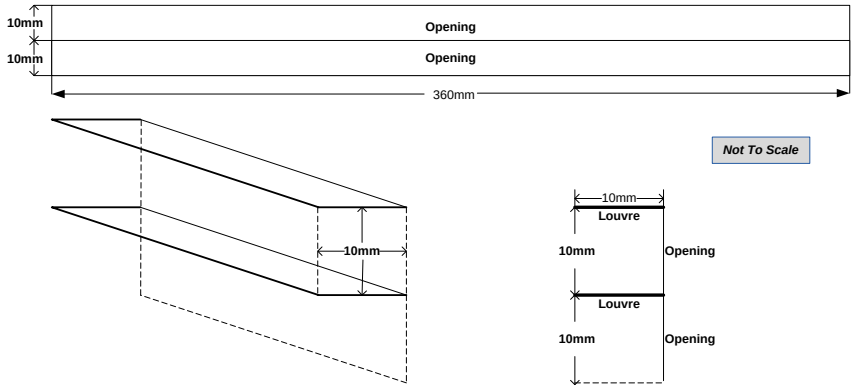

Figure 3 Louvre vent design and specification

A Brooks GF125 Digital Thermal mass flow controller (+/- 1.0% Flow Accuracy) supplied helium (A grade), used as a safe analogue for hydrogen, into the enclosure via a vertical 4mm diameter nozzle, centrally positioned 100 mm from the base of the enclosure, to simulate a leak from a fuel cell. Tests with plain vents and simplified louvre vents using helium leak rates from 1 to 10 nlpm was undertaken. Eight mini katharometer helium sensors (Xensor Ltd: TGC3880) were incorporated into the plywood enclosure to record gas dispersal behaviour. Two sensor arrangements were used. 'Frame sensors' comprised two horizontal lines of four sensors, mounted on a steel frame at heights of 345 mm and 555 mm above the enclosure floor, to establish and average helium concentration in the upper part of the enclosure. 'Stacked sensors' comprised a single vertical column of eight sensors positioned centrally near to an end wall at heights of 120, 225, 320, 420, 470, 535, 570 and 590 mm above the enclosure floor, to provide data on the vertical concentration gradient and stratification within the enclosure. The sensors record data sequentially at one second intervals, so take a reading every eight seconds. For each test the flow passed through the transient phase to steady state as shown in figure 4. To avoid the effect of the amplitude perturbations shown in the graph, a 100 second time averaged section of steady state data was taken to provide average helium concentrations following the methodology in [10].

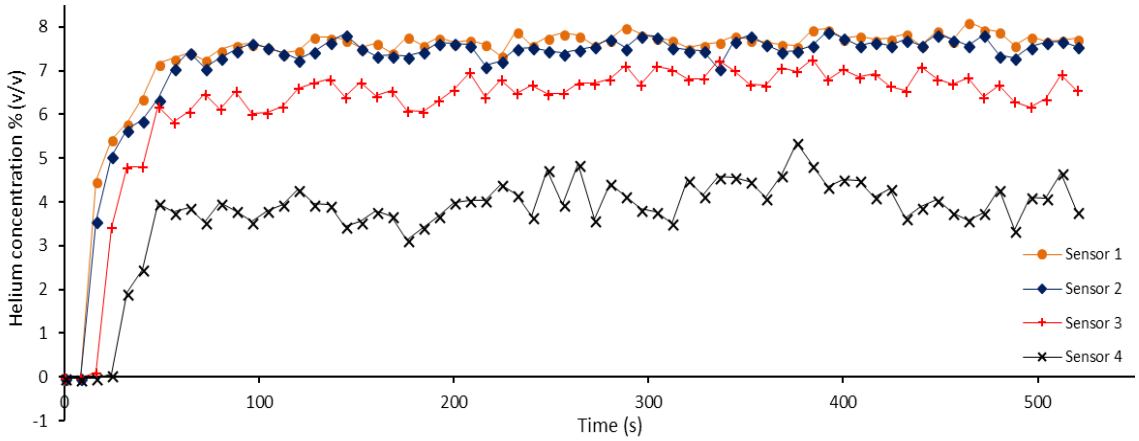

Figure 4 Time series for top four stack sensors using louvre vents at 10 lpm

2.1 Method: CFD Modelling

SolidWorks Flow Simulation CFD was used to model the experimental setups in this investigation. Flow Simulation solves the equations for the conservation of mass, momentum and energy for fluid flows, supplemented by fluid state equations, which define the nature of the fluid with regards to, for

example, fluid density, viscosity and thermal conductivity. It was developed to investigate the turbulent flows encountered in engineering. To predict turbulent flows, it uses the 'Favre-averaged Navier Stokes equations', where time averaged effects of flow turbulence on flow parameters are considered [11]. The *k–ε* transport equation for turbulent kinetic energy and its dissipation rate[12] are used to close the equations (1-6). Flow Simulation uses one system of equations to describe both laminar and turbulent flows and transition from a laminar state to a turbulent state and vice versa is possible. Equation 7 is the function that allows for laminar-turbulent transition [11].

$$\frac{\partial \rho k}{\partial t} + \frac{\partial}{\partial x_i}(\rho u_i k) = \frac{\partial}{\partial x_i}\left(\left(\mu + \frac{\mu_t}{\sigma_k}\right)\frac{\partial k}{\partial x_i}\right) + S_k \quad [1]$$

$$\frac{\partial \rho \varepsilon}{\partial t} + \frac{\partial}{\partial x_i}(\rho u_i \varepsilon) = \frac{\partial}{\partial x_i}\left(\left(\mu + \frac{\mu_t}{\sigma_\varepsilon}\right)\frac{\partial k}{\partial x_i}\right) + S_\varepsilon \quad [2]$$

$$S_k = \tau_{ij}^R \frac{\partial u_i}{\partial x_j} - \rho\varepsilon + \mu_t P_B \quad [3]$$

$$S_\varepsilon = C_{\varepsilon 1}\frac{\varepsilon}{k}\left(f_1 \tau_{ij}^R \frac{\partial u_i}{\partial x_j} + \mu_t C_B P_B\right) - C_{\varepsilon_2} f_2 \frac{\rho\varepsilon^2}{k} \quad [4]$$

$$P_B = \frac{G_i}{\sigma_B}\frac{1}{\rho}\frac{\partial p}{\partial x_i} \quad [5]$$

$$\mu_t = f_\mu \frac{C_\mu \rho k^2}{\varepsilon} \quad \text{(Turbulent eddy viscosity)} \quad [6]$$

$$f_\mu = \left[1 - exp\left(-0.0165 R_y\right)\right]^2 . \left(1 + \frac{20{,}5}{R_T}\right) \quad \text{(Turbulent viscosity factor)} \quad [7]$$

$$\text{Where } R_T = \frac{\rho k^2}{\mu\varepsilon}, \quad R_y = \frac{\rho\sqrt{k}y}{\mu}, \quad f_1 = 1 + \left(\frac{0.05}{f_\mu}\right)^3, \quad f_2 = 1 - \exp(R_T^2) \quad [8]$$

The constants are C_μ = 0.09 C_{ε_1} = 1.44 C_{ε_2} = 1.92 σ_ε =1.3 σ_k =1, C_B = 1 if $P_B > 0$ and 0 otherwise.

SolidWorks design software was used to develop a computer aided design (CAD) solid geometric model of the fuel cell enclosure, containing all the wire frame, surface geometry required to describe the edges and faces required for a CFD simulation [11]. Horizontal vanes were applied to the openings for the louvre tests. This model was configured to simulate the empirical test conditions. The enclosure CAD model was placed within a computational domain the same size as the external rig housing used in the empirical tests. The simulation in these tests is modelling flow through the enclosure and the wider computational domain, which allows flow through the vents to be modelled explicitly. A volume flow inlet condition is applied to the horizontal top surface of the helium nozzle to reflect the leak rate. When the simulation is set up, a basic parallel piped cuboid 'initial' mesh, orthogonal to the Cartesian axes, is created in the computational domain. Mesh settings can refine the whole mesh density or for areas of interest, a 'local initial mesh' can be created using additional geometry (later disabled) which is meshed independently. This approach was adopted in this study, where a cone was added in the plume and a cuboid in the area of likely stratification. Mesh sensitivity was tested using three levels of refinement, with the most refined being selected.

3.0 Results and discussion

Four sets of tests were completed-experimentally and numerically;

- Plain vents with frame sensors
- Plain vents with stacked sensors
- Louvre vents with frame sensors

- Louvre vents with stacked sensors

Plain vent tests provide a standard against which to measure louvre vent performance.

3.1 Experimental results: Plain Vents-Frame sensors

The frame sensor results for the plain vent test are shown in figure 5. Figure 5 (a) shows a distinct difference in concentrations achieved by the sensors on the upper and lower bars of the frame. The lower bar at 345 mm does not exceed 0.3 % at the highest leak rate and the top bar at 555 mm achieves a maximum of 5.73 % at 10 lpm, with the LFL achieved at 6 lpm. The maximum average concentration of all the sensors is 2.86 % at 10 lpm.

The much higher concentrations present at the top level clearly indicates the buoyant nature of the gas and the build-up of helium in the upper part of the enclosure suggests that stratification may be present. A further point of interest is the change of gradient at 3 lpm in figure 5 (a) for sensors 1 to 4 and also in figure 5 (b) from 3 lpm, the increase in concentration at each leak rate increase, is much reduced from that found between 1 lpm and 2 lpm and between 2 lpm and 3 lpm. This may be due to the helium leak developing from a weak plume to a stronger plume or more of a jet as the leak velocity increases.

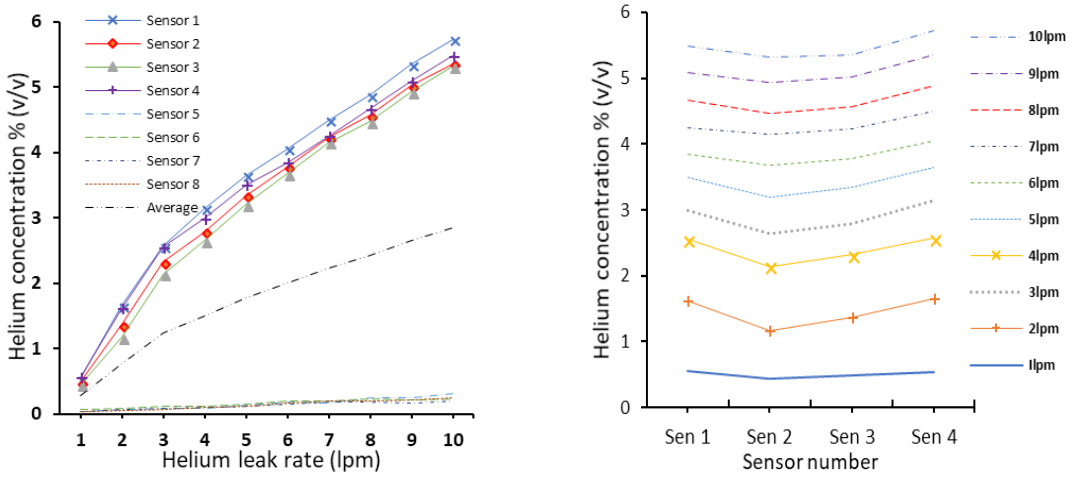

(a) **(b)**

Figure 5 Frame sensor helium concentrations (a) for all sensors (b) at the 555 mm level

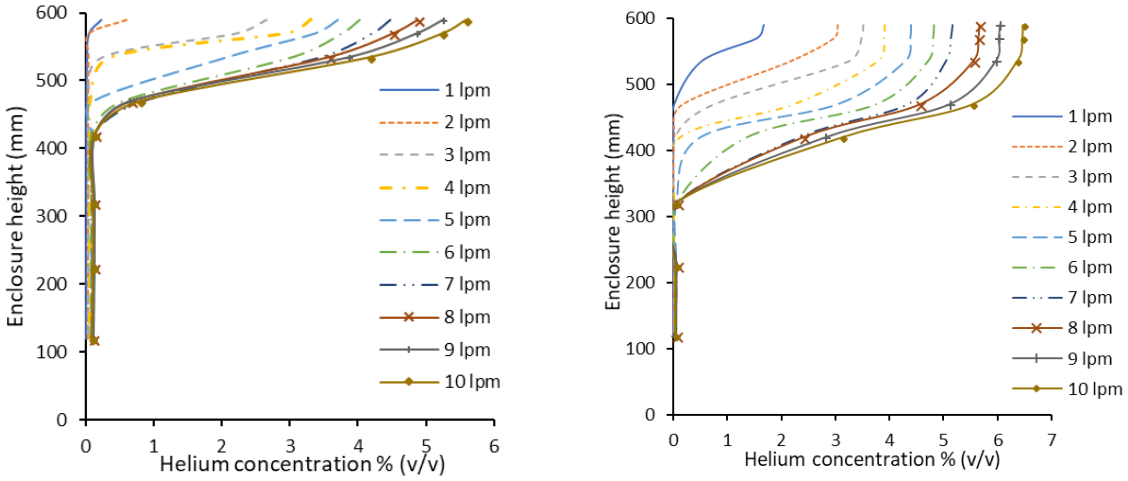

(a) **(b)**

Figure 6 Stacked sensor helium concentrations against height (a) Plain vents (b) Louvre vents

3.1.1 Plain Vents-Stacked sensors

Figure 6(a) presents the plain vent enclosure results with stacked sensors and Figure 6(b) the louvre vent stacked sensor results, discussed in section 3.2.4. The stacked sensor arrangement provides more

information about the enclosure concentration gradient and how it changes with height at each leak rate. With plain vents a distinct stratified layer is very evident in the enclosure, particularly from 3 lpm upwards. Concentrations above 4% (the LFL) are present above about 500mm and from 6 lpm upwards.

The displacement ventilation scheme has created the predicted stratified layer at the top of the enclosure. This layer gradually thickens, and stratified layer concentrations increase as the helium leak rate increases. Of note again is the change in behaviour at 3 lpm. There is a clear development in the regime inside the enclosure with a significant increase in helium concentration in the stratified layer.

3.1.2 Louvre Vents-Frame sensors

Figure 7 (a) shows the graph for helium concentration against leak rate for the louvre vented enclosure using frame sensors. The trends presented are similar to those found with the plain vents (Figure 5), but the concentrations at the top row of sensors are higher, peaking at 6.03 % for the 10 lpm leak rate. Sensors 7 and 8 on the lower row have also recorded slightly higher concentrations as the leak rate increases. A change of gradient is again apparent from 3 lpm.

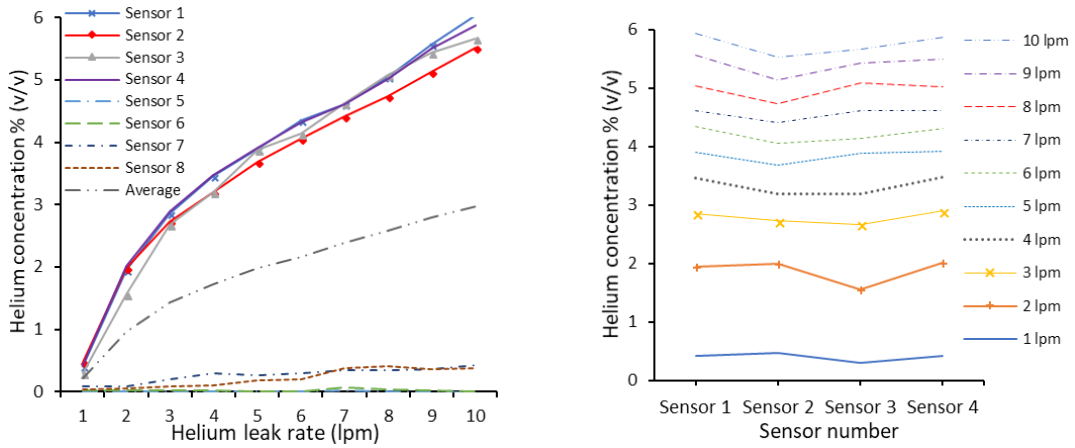

(a) **(b)**

Figure 7 Frame sensor helium concentrations (a) for all sensors (b) at the 555 mm level

3.1.3 Louvre Vent-Stacked sensors

The results in Figure 6(b) for louvre vents and stacked sensors show that a distinct stratified layer is present for all leak rates. The LFL is exceeded at 5 lpm (7 lpm for plain sensors) and all leak rates produce concentrations exceeding 25 % of the LFL in the stratified layer. The addition of two horizontal louvres has changed the ventilation regime present in the enclosure. The louvres would appear to be reducing the flow rate through the vents causing the helium to 'back-up' and build a thicker layer at the top of the enclosure, than was experienced with plain vents.

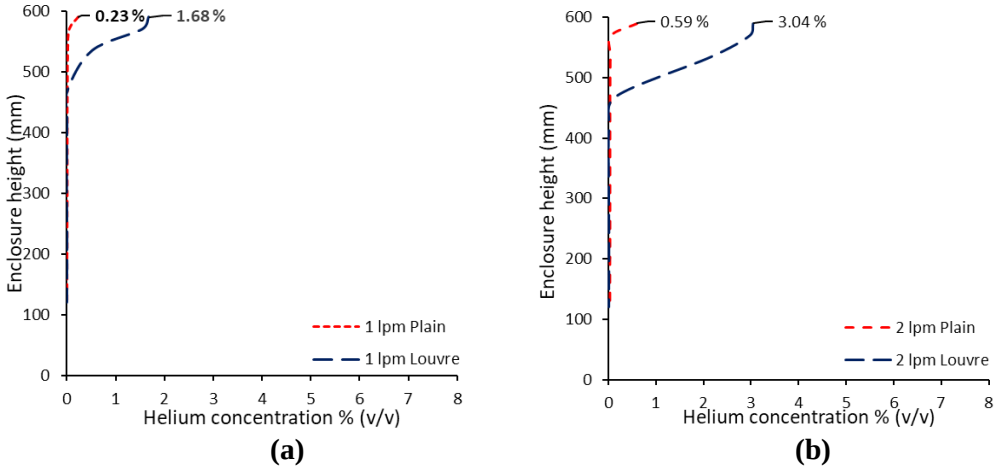

(a) **(b)**

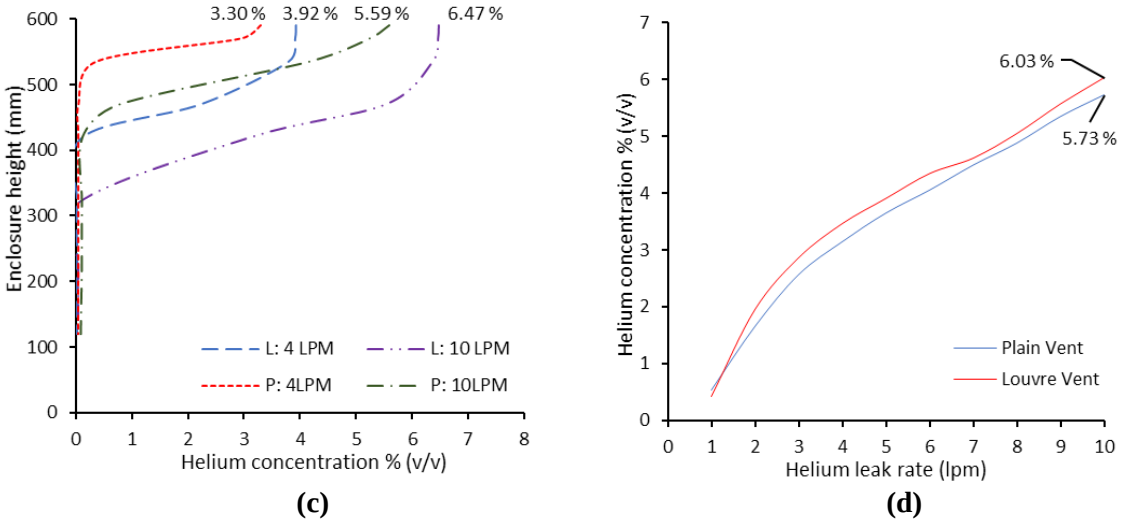

Figure 8 Comparison of plain (P) and louvre (L) vent (stacked sensor) concentrations at (a) 1 lpm, (b) 2 lpm, (c) 4 and 10 lpm and (d) Frame sensor concentrations at sensor 1 (Peak concentrations shown on graph)

Figure 8 (a) shows a comparison of stacked sensor readings for plain and louvre vents at 1 lpm and 8 (b) at 2 lpm. Although the LFL is not exceeded at these leak rates, the increase in high-level concentration is quite marked with the addition of louvres on the vent opening. At 1 lpm the peak concentration goes from 0.23 to 1.68 % and at 2 lpm the peak concentration jumps from 0.59 to 3.04 %, an increase of almost 2.5 percentage points. Figure 8 (c) compares enclosure helium concentrations using plain and louvre vents at 4 and 10 lpm. In both instances the addition of louvres has increased helium concentrations in the stratified layer, by 16.66 % (at 4 lpm) and 15.12 % (at 10 lpm). Figure 8(d) shows the difference in plain and louvre vent concentrations at frame sensor position 1. Apart from at 1 lpm, the addition of louvres has led to an increase in helium concentration.

3.2 CFD results (SolidWorks: Flow Simulation):

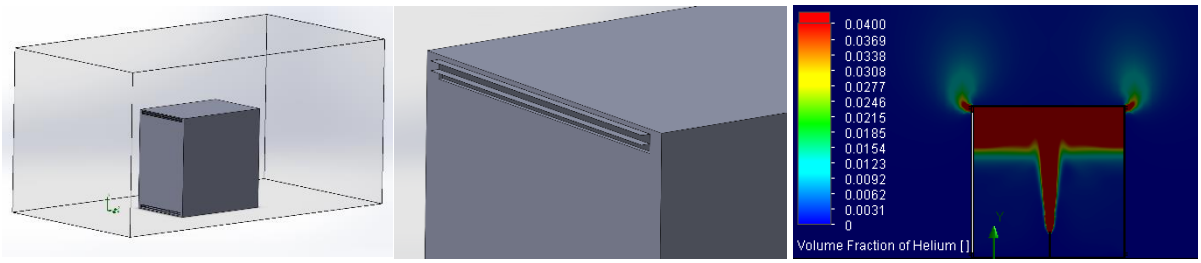

(a) (b) (c)

Figure 9 SolidWorks Flow Simulation images (a) Enclosure (b) Louvres (c) Cut plane at 10lpm

Two simplified CAD models were created in SolidWorks (Figure 9(a)), one with plain vents and one with louvre vents (Figure 9 (b)). A computational domain equivalent to the outer enclosure was created and a series of simulations were run at leak rates from 1 to 10 lpm. Point source data was then extracted for helium concentration at the equivalent experimental sensor positions. Figure 9(c) is an example cut plot of helium concentration in the enclosure, showing the helium plume and stratified zone.

3.2.1 Plain Vents-Frame sensors

Figure 10 presents the frame sensor CFD concentration data. The overall trends in terms of increasing concentration with increased leak rate are similar to those for the experimental data in figure 5. The simulations have reproduced the flow behaviour seen experimentally with similar concentrations.

Differences are that CFD helium concentrations are higher for the top sensor positions at low leak rates, and CFD top sensor concentrations at higher leak rates are lower than with the empirical data.

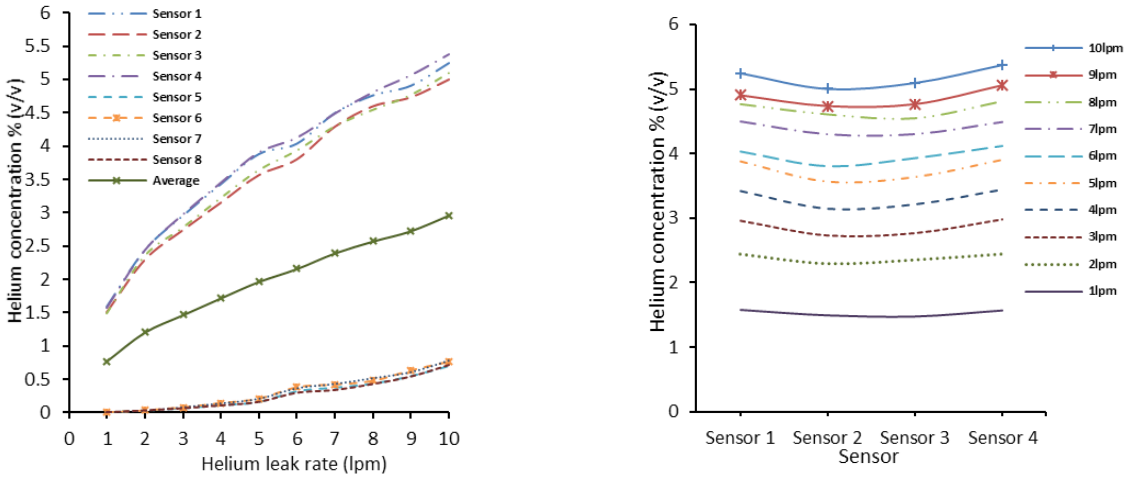

(a) **(b)**

Figure 10 Frame sensor helium concentrations (a) for all sensors (b) at the 555 mm level

3.2.2 Plain Vents-Stacked sensors

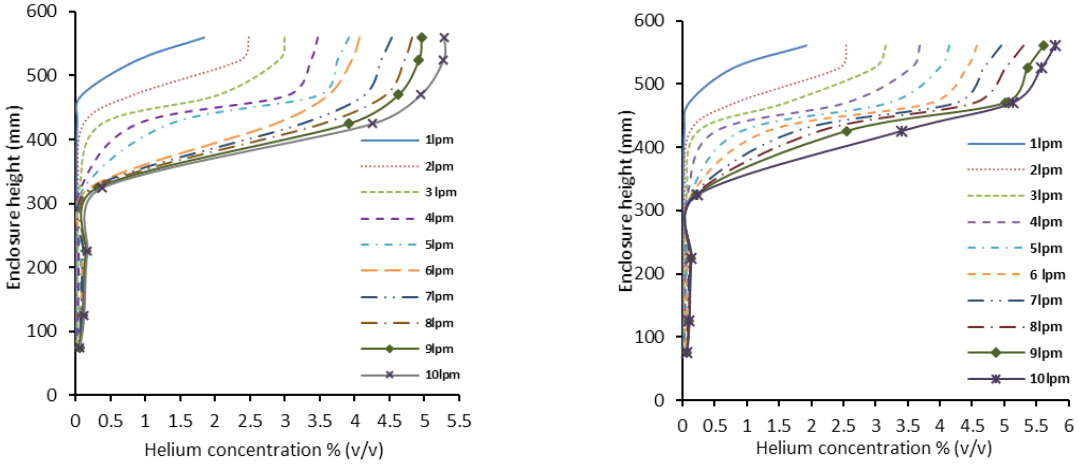

(a) **(b)**

Figure 11 Stacked sensor helium concentrations against height (a) Plain vents (b) Louvre vents

Figure 11(a) presents the plain vent enclosure CFD results with stacked sensors and Figure 11(b) the louvre vent stacked sensor results, discussed in section 3.2.4. The trends produced by the experimental data of increasing concentration with height are reflected in the CFD data. The LFL is exceeded at the 6lpm leak rate, which is the same as for the empirical data. The maximum achieved is 5.29% at 10lpm (5.59 % for empirical data), and the depth of the stratified layer is deeper across the leak rate range. The 1 and 2lpm data series also both exceed the 1% (25% of LFL) mark, whereas the empirical data did not.

3.2.3 Louvre Vents-Frame sensors

Figure 12(a) presents frame sensor CFD data for concentration against leak rate. The trends presented are similar to those found with the experimental data in figure 7, with flow behaviour replicated and similar concentrations. The LFL is exceeded by the top sensor positions with the 5 lpm leak rate, whereas it was at 6lpm with the empirical data. Concentrations are marginally higher than the CFD data for plain vents but are slightly lower than the empirical data. Bottom sensor point data is also lower than for CFD plain vents, notably so at the higher leak rates. Figure 13 compares the CFD plain and louvre vent data at sensor 4. It shows that as the helium leak rate increases the louvre vent enclosure

concentration is higher than for that found with the plain vent enclosure. The model has identified additional flow resistance leading to a concentration increase.

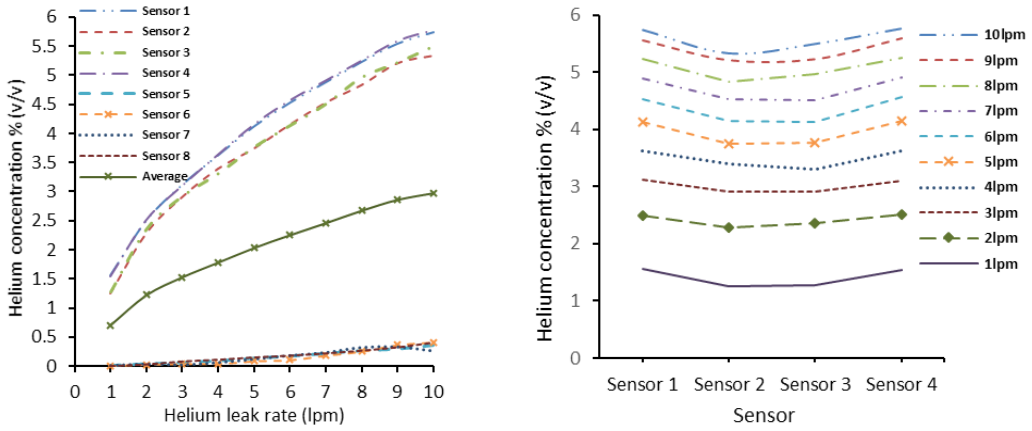

(a) **(b)**

Figure 12 Frame sensor helium concentrations (a) for all sensors (b) at the 555 mm level

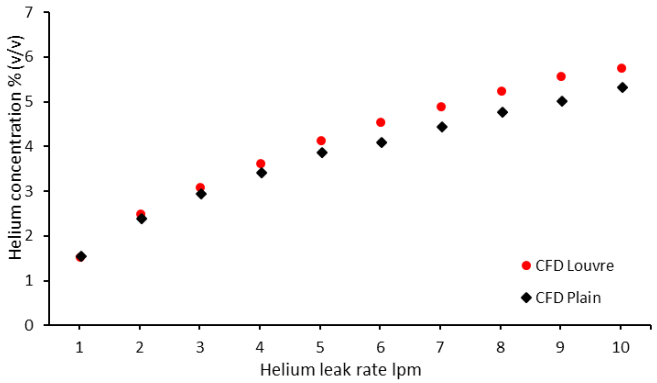

Figure 13 Comparison of CFD plain and louvre vent data at frame sensor 4

3.2.4 Louvre Vents-Stacked sensors

Figure 11 (b) presents louvre vent CFD data for enclosure height against helium concentration. The experimental trends of increasing concentration with height are present, but with slightly lower concentrations. The LFL is exceeded at 5lpm (6lpm for CFD plain vent tests and 5 lpm for experimental louvre vents tests). The depth of the stratified layer appears slightly shallower than for the CFD plain vent data in figure in figure 11(a), which is the opposite to what was found with the experimental tests.

3.2.5 Comparison of experimental and CFD data

The CFD validation exercise produced qualitative results that suggested the model was behaving in the way expected. Some of the CFD tests predicted helium concentrations that were at variance with the empirical tests, but in some cases the predictions were very close. Figure 14 compares the CFD and experimental frame sensor data at sensor 4. The correlation between the two data sets is very good with most variance at low leak rates.

Figure 15 (a) compares the CFD and empirical plain vent stacked sensor results at 10 lpm. The correlation is very good apart from in the stratified zone where the CFD has slightly under-predicted. In figure 15 (b) the peak concentrations are close, but the CFD has produced a shallower stratified zone. Figure 16 (a) compares CFD and experimental plain vent data for the stacked sensors at 4 lpm. The peak CFD concentration is slightly higher than with the experimental data and the CFD produces a deeper stratified zone. In figure 16 (b) the louvre data is compared. Again the peak concentrations are close but, on this occasion, the experimental data has a deeper stratified zone.

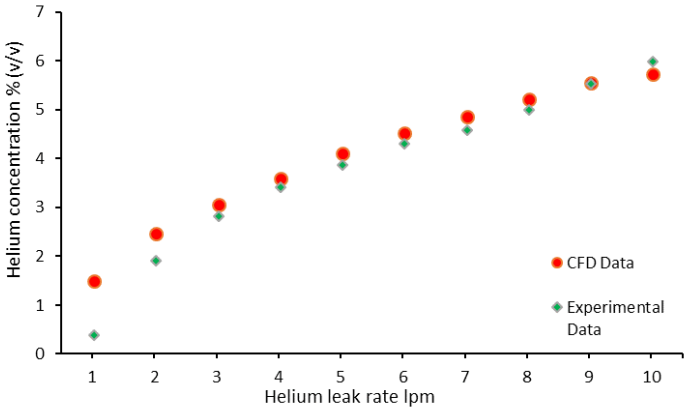

Figure 14 Comparison of CFD and experimental data at frame sensor 4

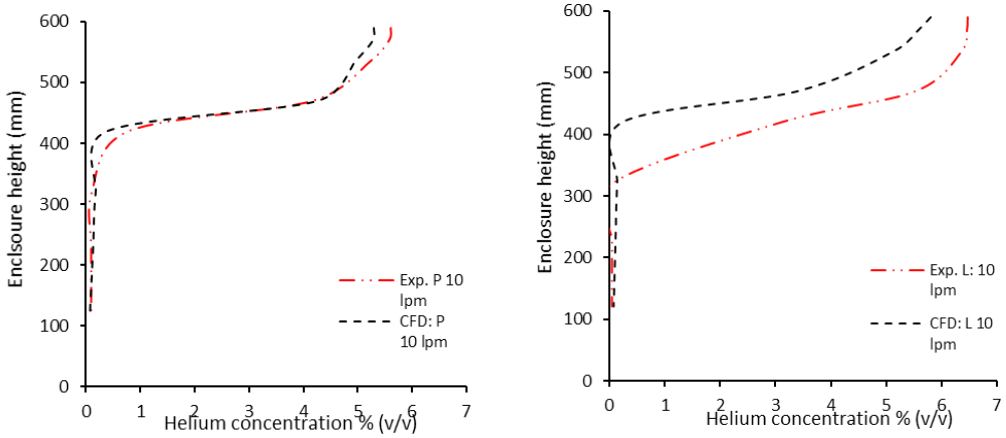

(a) **(b)**

Figure 15 Comparison of CFD and experimental data (a) plain and (b) louvre vents at 10 lpm

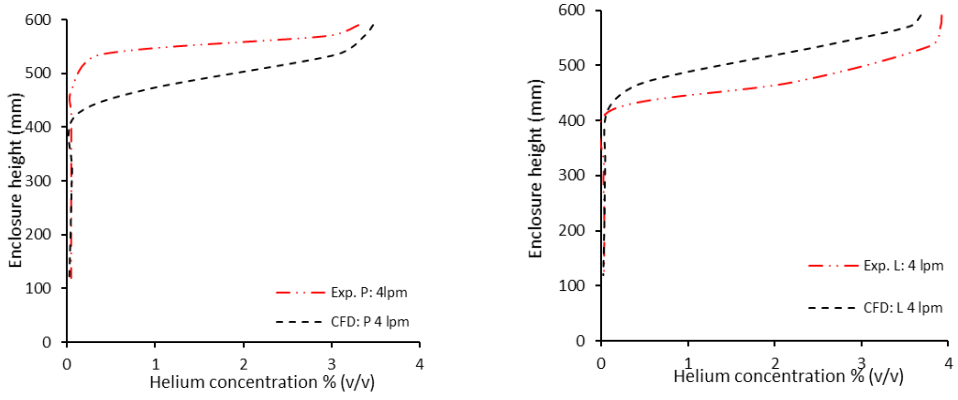

(a) **(b)**

Figure 16 Comparison of CFD and experimental data (a) plain and (b) louvre vents at 4 lpm

4.0 Conclusion and future work

This study has considered low-level helium leaks in a small fuel cell enclosure to understand when flammable levels are achieved. Empirical data shows that adding simple louvres to the plain vent openings increases helium concentrations in the stratified zone, which is also deeper, therefore increasing the volume in which a flammable mixture may be formed. At a leak rate of 10 lpm for the peak concentration, the relative percentage difference between plain and louvre vent performance is 14.6 %. For this leak rate at the 4 % concentration point the relative percentage difference in stratified depth is 19.5 %. Louvres increase flow resistance through the enclosure, so direct replacement of plain vents with same opening area louvre vents will not achieve the same performance, larger louvre vents would be necessary. The CFD predictions produced some good results with excellent correlations as

shown by figures 14 and 15(a). Generally, peak concentrations were close, but with some variation in stratified depth. A comparison of experimental and CFD results using relative percentage difference showed that with;

- Plain vent experimental and CFD data peak concentrations at 10 lpm: rpd = 6.0 %
- Plain vent experimental and CFD data at 10 lpm, stratified depth at 4% point: rpd = 0 %
- Louvre vent experimental and CFD data peak concentrations at 10 lpm: rpd = 11.1%
- Louvre vent experimental and CFD data at 10 lpm, stratified depth at 4 % point: rpd = 9.1 %

These findings support the use of SolidWorks Flow Simulation in this field and contribute towards validating its capability. Future enclosure investigations will test proprietary aluminium louvre vents.

Acknowledgements
The authors would like to acknowledge Sellafield Ltd. and BOC Ltd. for their support of this project.

Funding sources
Sellafield Ltd. Co-sponsored this project with London South Bank University, providing finds for experimental work. BOC Ltd. provided SolidWorks Flow Simulation CFD software.

Highlights
- Passive ventilation tests comparing plain rectangular vents and vents with louvre vanes
- Louvre vents shown to impede passive ventilation flow through the enclosure
- Louvre vents shown to increase stratified level buoyant gas concentrations
- SolidWorks Flow Simulation CFD validation exercise

References
1. Weiner S.C. (2014); Advancing the hydrogen safety knowledge base; International Journal of Hydrogen Energy; 39, 20357-20361
2. Molkov V. (2012); Fundamentals of hydrogen safety engineering. www.bookboon.com
3. Giannissi et al (2016); Mitigation of buoyant gas releases in single-vented enclosure exposed to wind: Removing the disrupting wind effect; International Journal of Hydrogen Energy; 41(6), 4060-4071
4. Liddament, M.W. (1996); A Guide to Energy Efficient Ventilation; Air Infiltration and Ventilation Centre, IEA Energy Conservation in Buildings and Community Systems Programmed; Coventry
5. Linden PF. (1999), The fluid mechanics of natural ventilation. Annual Rev Fluid Mech, 31, 201-38.
6. Brown WG, Solvason KR. (1962), Natural convection heat transfer through rectangular openings in partitions. Part I: vertical partitions. Int J Heat mass Transfer, 5, 859-68
7. Molkov, V., Shentov, V, Quintiere (2014): Passive ventilation of a sustained gaseous release in an enclosure with one vent; International Journal of Hydrogen Energy; 39, 8158-8168
8. Hübert, T.; Boon-Brett, L.; Black, G.; Banacha, U. (2011); Hydrogen sensors – A Review; Journal of Sensors and Actuators B: Chemical; 157, 329–352
9. Bachellerie, E.; Arnould, F.; Auglaire, M.; de Boeck, B.; Braillard, O.; Eckardt, B.; Ferroni, F.; Moffett R. (2003); Generic approach for designing and implementing a passive autocatalytic recombiners PAR-system in nuclear power plant containments; Journal of Nuclear Engineering and Design; 221, 151–165.
10. Cariteau, B., Tkatschenko, I. (2013); Experimental study of the effects of vent geometry on the dispersion of a buoyant gas in a small enclosure; International Journal of Hydrogen Energy; 38, 8030-8038
11. Dassault Systemes (2015 (a)); Technical Reference; SolidWorks Flow Simulation 2015
12. Launder, B.E. and Spalding, D.B. (1974), The numerical computation of turbulent flows: Computational methods in applied mechanical engineering, 3, 269-289